Direct experimental comparison between tomo-PIV and scanning tomo-PIV: wake flow behind a half-cylinder

Lionel Thomas, Benoit Tremblais, Patrick Braud, Laurent David

10TH INTERNATIONAL SYMPOSIUM ON PARTICLE IMAGE VELOCIMETRY - PIV13
Delft, The Netherlands, July 1-3, 2013

Direct experimental comparison between tomo-PIV and scanning tomo-PIV: wake flow behind a half-cylinder

L. Thomas[1], B. Tremblais[2], P. Braud[1] and L. David[1]

[1] Institut Pprime, CNRS . Université de Poitiers . ENSMA - UPR 3346
Département Fluides, Thermique, Combustion - Axe HydÉE
Bâtiment H2 - SP2MI Téléport 2
Boulevard Marie et Pierre Curie - BP 30179
F86962 FUTUROSCOPE CHASSENEUIL Cedex
contact: lionel.thomas@univ-poitiers.fr

[2] Institut XLIM-SIC
Université de Poitiers
Téléport 2, avenue Clément ADER BP 40109
F86961 Futuroscope Chasseneuil

ABSTRACT

In this paper, a direct experimental comparison is made between scanning and tomo-PIV, on an unsteady wake flow behind a half-cylinder. Several seeding densities are used in order to demonstrate the capacities and limitations of both techniques. For the scanning technique, the effect of particles elongation is investigated and the influence of the seeding density on the volume reconstruction for tomo-PIV is examinated. The results of the two techniques are compared in terms of volume and velocity fields.

1. Introduction

In the literature, many studies have been carried out on the flow around a cylinder with tools for measuring the two components or the three components of the velocity [12]. Nevertheless, this classic flow is complex and sensitive to the Reynolds number. Recently for low Reynolds numbers different configurations have been tested to control the flow by using a half cylinder to fix the separation points or by adding a splitter plate to reduce the vortex shedding and the drag [10]. The 3D effects seem to have some influence on the wake and we propose to measure this flow by means of 3D diagnostics. Several methods are currently used to measure the three components of the velocity field in a volume. Holography [6], tomo-PIV [3], [11], scanning-PIV [5], 3D-PTV [7] and [8] among others are powerful tools to get three-dimensional measurements. In this paper, only tomo-PIV and scanning-PIV are considered and are used simultaneously to validate the algorithms of tomography PIV with a technique of scanning. A direct experimental comparison between the two techniques is performed, which is usually technically difficult. This comparison gives access to a direct validation of the reconstruction technique in a real case which is more realistic that the previous validation made with a solid block by these two techniques [4]. Some effects are particularly investigated like the seeding density and the particle elongation for the scanning. The results of the two techniques are compared in terms of volume and velocity fields.

2. Experimental setup

The flow investigated is a laminar wake behind a half-cylinder. The experimental setup is presented in figure 1. Two pumps supplies water to a close-loop system. A big tank is imposing the pressure inside the water channel. The flow is regulated using small pipes and two grids. The Reynolds number is around 300, based on the diameter of the half cylinder and the mean stream velocity. The cylinder diameter was 20 mm and the channel was 160×160 mm^2 squared. The fluid used is water at $20°\mathcal{C}$. The flow was seeded using $21\mu m$ particles of polyamid (ρ=1.04 g/cm^3). The volume was illuminated with a Nd:YLF 10 kHz quantronix laser. The laser sheet was 1 mm thick. The measurement volume was 30 mm thick and generated using high speed scanning. The measurement volume is presented in figure 2. One high speed 1024×592 camera (cam5) is used for the scanning-PIV technique and four 1600×1200 cameras (cam1, cam2, cam3 and cam4), opened during all the laser sheet volume scanning, are used for the tomo-PIV. The configuration of the cameras is presented in figure 3. The calibration of the cameras was performed using a paper calibration grid, shifted through the whole measurement volume. Different seeding densities were used, defined by the mass of particles added in the water tank. 0, 1, 2, 3, 4, 5, 6, 8 and 10 grams were tried.

3. Data processing

All the codes used to process the data were developed using the SLIP C++ library [14].

3.1 TOMO-PIV

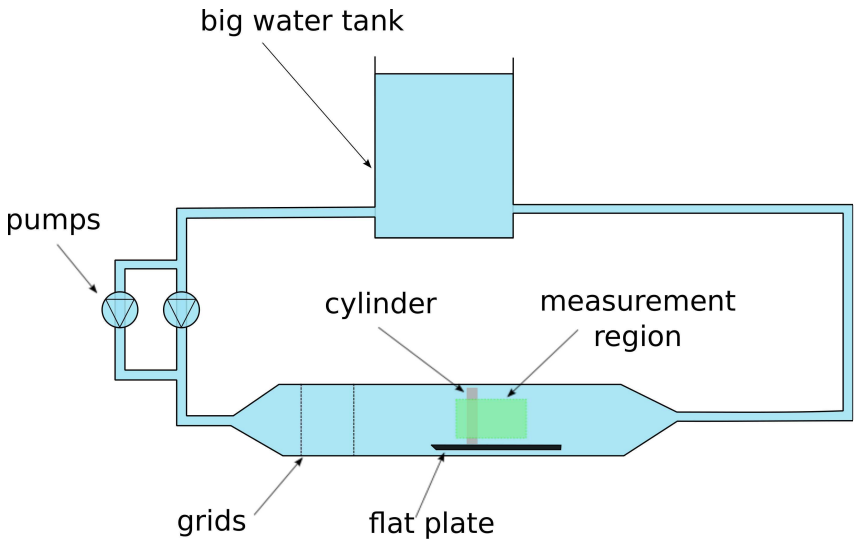

Figure 1: Experimental setup.

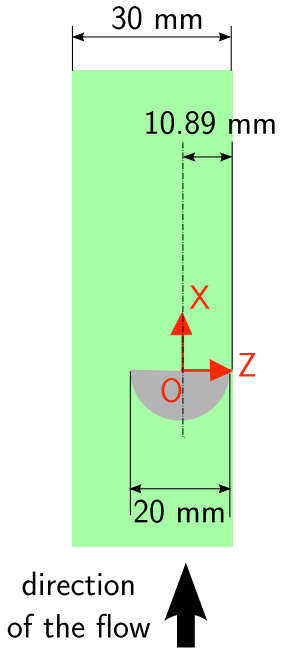

Figure 2: Top view of the cylinder and the measurement volume.

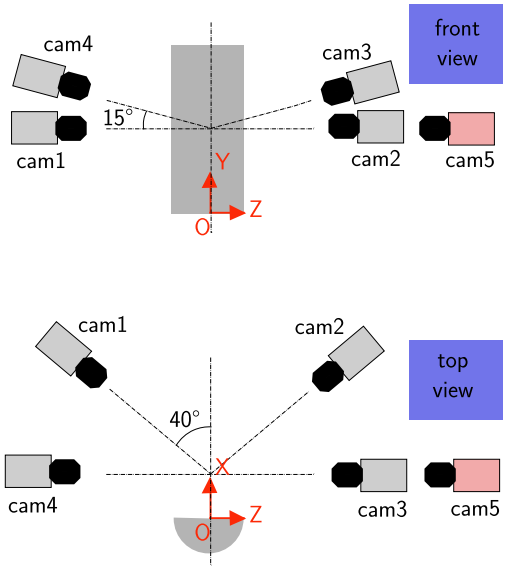

Figure 3: Cameras configuration.

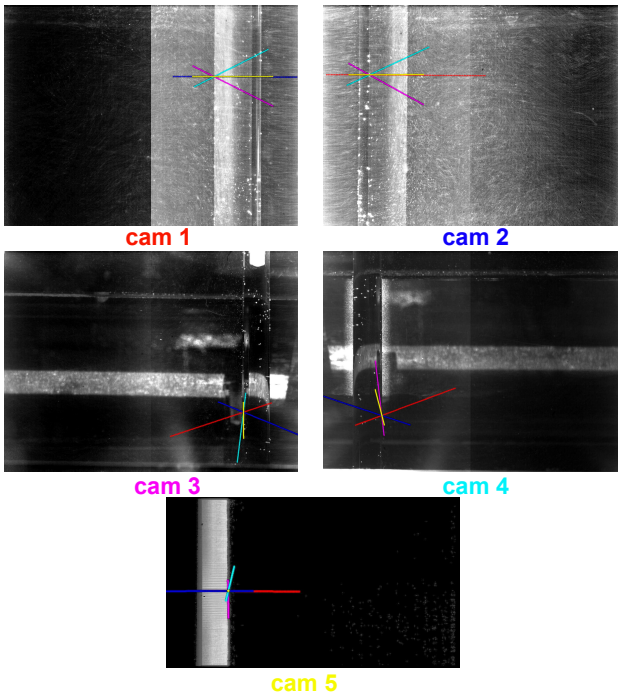

Figure 4: Image of the cylinder and lines of sight coming from the different cameras and going through the same bubble.

The background of the images was removed subtracting a background image computed using a size 20 temporal median filter. The cameras were calibrated using a calibration target displaced along a direction perpendicular to the laser sheet. Nine positions were used to fit a pinhole camera model for each camera. A specific self-calibration procedure was used to be sure that all the cameras are correctly aligned. Each volume obtained with the scanning technique was projected on cam5, in order to get a fifth tomo-PIV image, used as a reference during the misalignment procedure. Cameras 3, 4 and 5 were being fixed on a tripod. The self-calibration procedure was working easily for these three cameras. The two other cameras were being fixed on a rigid structure, and the heavy calibration target was fixed on it, deforming the structure, and then moving the cameras. Hence, problems arose during the self-calibration procedure for these cameras. The misalignment errors were to large to be corrected with the standard procedure. The camera models were then shifted manually before applying the misalignment correction. This shift was evaluated using bubbles staying along the cylinder that were being visible on all tomo-PIV cameras. The result of the bubble line-of-sight crossing is shown in figure 4. Essentially a 19 mm shift was applied in the Y direction.

The 0g seeding images were used to perform the self-calibration. The maximum misalignment error was 3.6 pixels and after correction, it was lower than 0.1 pixels.

The reconstruction was performed using 8 BIMART iterations. The BIMART algorithms is a expansion of the MART algorithm family and is presented in [13] and [1]. The volumes size is $890\times600\times300$. The voxel physical size is 0.1 mm. The difficulty here was to choose the best seeding density in order to get the best reconstruction result. Our criterion to achieve this was to take the velocity field leading to the smallest divergence RMS value. This quantity has been already used to assess a velocity field quality (see [9]). The velocity field was obtained with a $64\times64\times64$ final interrogation window size, with a first pass using $128\times128\times128$ interrogation windows.

The results concerning the divergence RMS value are presented in figure 5. Two particle densities give a minimum divergence RMS

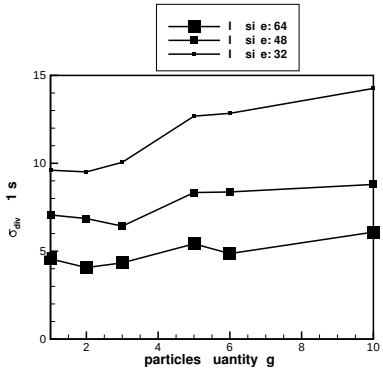

Figure 5: Evolution of the divergence RMS value, as a function of the particles quantity and the final interrogation window size.

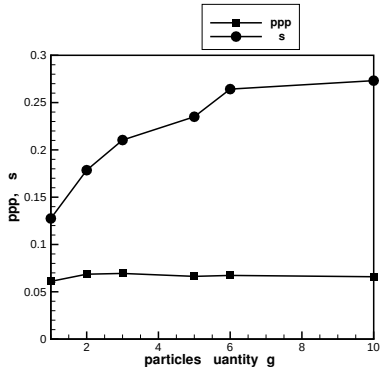

Figure 6: Evolution of the evaluated particle per pixel (ppp) and the image signal ratio (Ns).

value. For the biggest interrogation windows, the optimal particle quantity is 2 grams, while for the intermediate interrogation window size, 3 grams is slightly better. The smaller the interrogation window, the higher the particle quantity. Anyway, above a certain concentration, the result quality decreases. Other quantities characterizing the particle density are interesting to investigate: the number of particles per pixel (ppp), and the image signal ratio (Ns). It is clear from figure 6 that the image is saturated above a particle quantity corresponding to 2 grams of particles put in the tank. This justifies also that the reconstruction should be the best around this particle concentration, as the images begin to saturate, particles hiding each other. As there are four cameras, ambiguities can be eliminated in some way if the saturation if not very high. Ns values are low for such ppp: a gaussian filter applied on the images can improve the reconstruction quality in this case.

3.2 Scanning-PIV

The volumes are generated from the stacked images. The images are dewarped using the camera model. After volume reconstruction, the voxels are not cubic: they are three times more elongated along the Z direction. The volumes are interpolated on the same regular grid as used in tomo-PIV. The resulting volume contains elongated particles, which are the result of the convolution of the spherical particles intensity profile with the laser sheet profile. The deconvolution problem is not an easy one, and in this paper, a simple technique has been tried in order to evaluate the effect of this elongation of the particles. The volume has been filtered in order to reduce this elongation. This filter consists in detecting all the particles in the volume and replacing them with a spherical particle, with a gaussian intensity profile. The detection is performed looking for connected components after a global thresholding. The position is computed using centroid evaluation. The intensity and the variance of the particle are computed using statistics on the voxels inside the detected particle. Particles that are too small or too elongated are eliminated. The volumes are compared in image 7. The particles match quite well. All the significant particles are identified and replaced by spherical particles. Concerning the correlation of volumes obtained with scanning PIV, the best particle concentration is the highest. Indeed, no artifacts appears in the velocity field when the quantity of particles varies between 2 and 10 grams and using a high concentration, it is possible to decrease the final interrogation window size for the velocity fields computation. It is possible to go down to $32\times32\times32$ (and probably even less). The result on the velocity fields is shown in figure 9. A zoom around the cylinder is presented. This comparison shows that the main differences concerns the Z direction. Even if the velocity fields look very similar on a global point of view, there are some differences near the cylinder and inside the vortex. The velocity vectors follow better the cylinder wall upstream in the filtered case. In general, the differences on the w component of

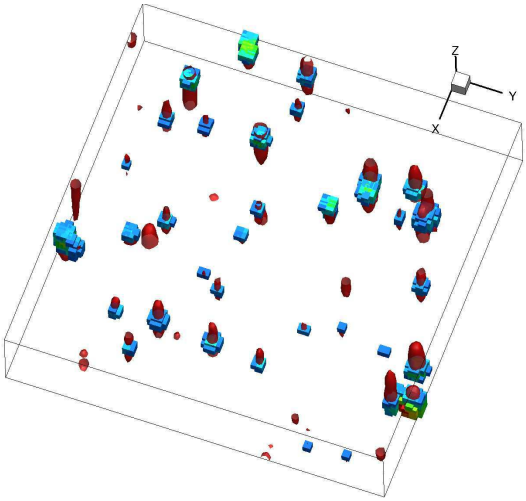

Figure 7: Comparison of the volumes (particle density corresponding to 2 grams) obtained with the scanning technique: the raw particles are presented smooth and in red, while the filtered particles are made from blue voxels.

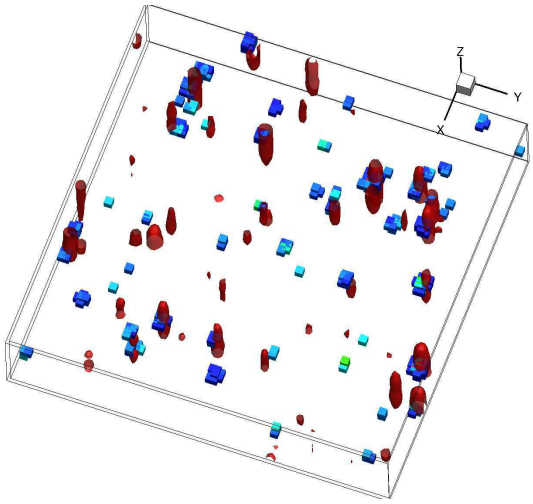

Figure 8: Comparison of the volumes (particle density corresponding to 2 grams) obtained with the scanning technique (smooth, red particles) and with Tomo-PIV (blue voxels).

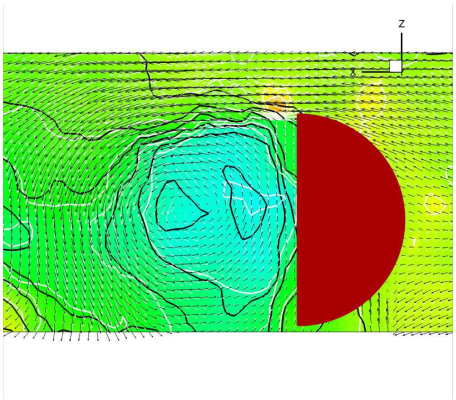

Figure 9: Comparison of velocity fields obtained with and without filtering (vector fields are tangent velocity fields, and lines are iso-w contours). The data without filtering is in black, while the data with filtering is in white. The cylinder is shown in dark red.

the velocity appear when this velocity component takes low values. The results seems to be slightly improved by the filtering, but it is probably possible to find a more sophisticated deconvolution technique.

4. Comparison of the techniques

The volumes are generated with the same resolution. A direct comparison of the volumes can be performed. Anyway, a real comparison can be performed only for low seeding densities as high seeding densities introduces too many ghost particles when using tomo-PIV. The comparison is performed for the tomo-PIV particle concentration (2 g). The result is shown in figure 8. There is a rather good correspondence between the particles. The differences are mainly due to the noise which is different in the fast cameras and the normal cameras, hence the background elimination technique and low level illumination on the fast camera can partially explain the differences. The velocity fields can also be compared, using $64\times64\times64$ final interrogation windows. The result is shown in figure 10. In this figure, the vectors are the projection of the velocity on the plane and the lines are the iso-contours of the perpendicular velocity component. These data are drawn in black for the scanning technique and in white for tomo-PIV. A very good correspondence is observed between the two techniques. Both vectors and lines match very well. The only big difference concerns the region upstream of the cylinder: the results for tomo-PIV are not accurate because the light goes through the cylinder and this is not modeled by the camera models. The same result can be presented in other planes (see figures 11 and 12). The same conclusion can be made about the correspondence of the techniques. Even in the Z direction, the velocity fields match closely.

5. Results

The best result is given by the scanning technique (giving a divergence RMS of 2.6 s^{-1}) because it is possible to get a higher spatial resolution. The main drawback of the technique is that the flow must be slow enough so that the flow can be considered as frozen.

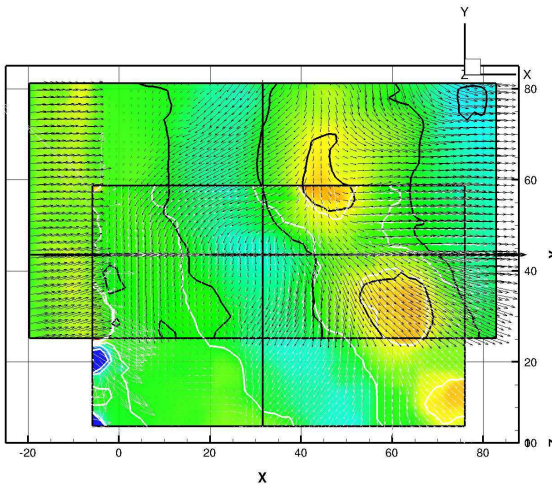

Figure 10: Comparison of the velocity fields obtained in the XY plane with scanning (in black) and tomo-PIV (in white). The velocity vectors represented are tangential ones and the lines are iso-contours of the perpendicular velocity component.

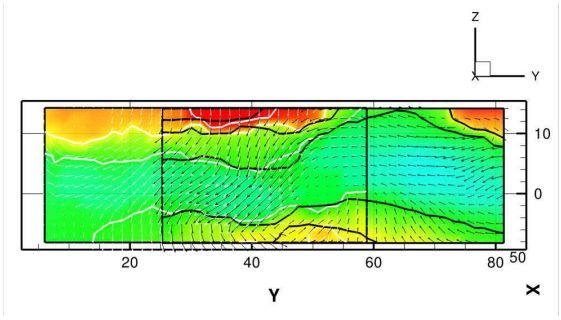

Figure 11: Comparison of the velocity fields obtained in the YZ plane with scanning (in black) and tomo-PIV (in white). The velocity fields represented are tangential and the iso-contours represents the velocity component perpendicular to the plane.

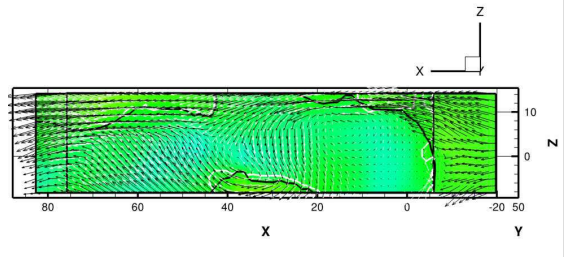

Figure 12: Comparison of the velocity fields obtained in the XZ plane with scanning (in black) and tomo-PIV (in white). The velocity fields represented are tangential and the iso-contours represents the velocity component perpendicular to the plane.

More precisely, that means that the equation (1) should be verified.

$$||\frac{\partial \mathrm{u}}{\partial t}|| \ll 2\frac{||\mathrm{u}||}{\Delta T} \tag{1}$$

where ΔT is the time interval between the beginning and the end of the scan. In our case, the measurements are time-resolved hence it is possible to check this condition by approximating the time derivative by finite differences, leading to equation (2).

$$\frac{||\mathrm{u}(t+\Delta t)-\mathrm{u}(t)||}{||\mathrm{u}(t+\Delta t)+\mathrm{u}(t)||} \ll \frac{\Delta t}{\Delta T} \tag{2}$$

where Δt is the time interval between the second and the first exposure. In the present experiment, $\frac{\Delta t}{\Delta T} = 2$. A computation of the ratio from the experimental data gives a maximum value around 0.25. That means that scanning-PIV is usable for the present flow. The temporal coherence of the technique is shown here through the consideration of figure 13 showing the temporal evolution of the Q-criterion iso-contours, colored by a vorticity direction index. The Q-criterion is computed robustly using some averaging around the point where it is computed. The temporal evolution is coherent. Large coherent structures parallel to the cylinder are clearly visible and form a Von Kármán vortex street. Some horizontal structures are also present. With this great experimental tool, it will be possible to better understand the physics of this flow.

6. Conclusion

In this paper, for the first time a direct experimental comparison between scanning and tomo-PIV is achieved. The scanning technique leads to better spatial resolution but it is limited to slowly varying flows. The elongation of the particles along the scanning direction due to a convolution between the particle intensity profile and the laser sheet profile reduce the measurement precision and a filtering of the particles, in case of very elongated particles, can be necessary. Tomo-PIV does not have restrictions on the velocity of the flow. However, the calibration procedure is crucial in order to get results, and the spatial resolution is limited by the reconstruction problems (linked to ghost particles). The choice of the seeding density is also important, even if it is possible to get proper results with

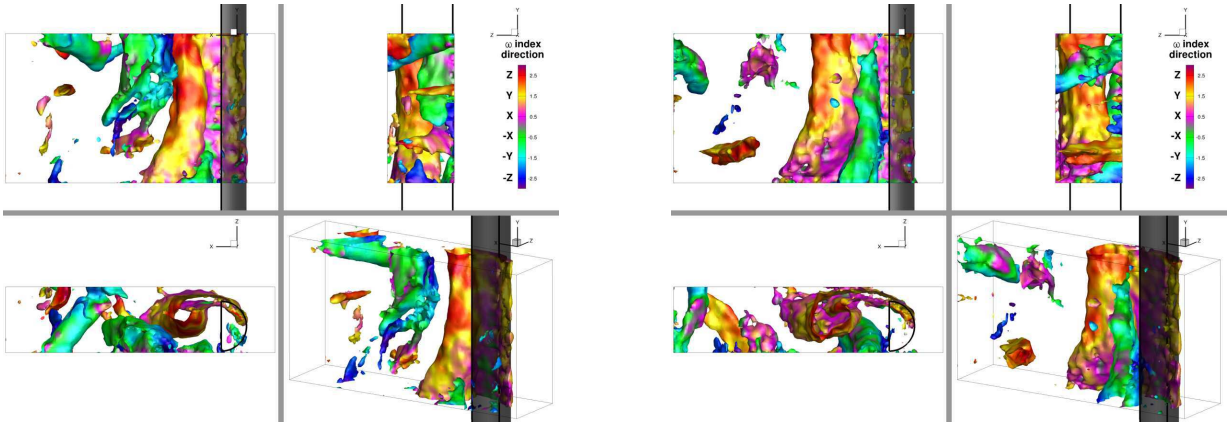

Figure 13: Example of Q criterion iso-values computed on the velocity field obtained with the scanning-PIV technique, for T=0 s (left) and T=2 s (right). Each instant contains four views. side view (top-left), top view (bottom-left), left-view (top-right) and 3d-view (bottom-right). The colors correspond to a vorticity direction index. For example, the green color means that the vorticity is in the -X direction.

rather different seeding densities. For a seeding density adapted to tomo-PIV, scanning-PIV and tomo-PIV leads to the same velocity field. This confirms that the volume reconstruction technique gives good results even on noisy experimental data. A good compromise between the two techniques is a combination of scanning and tomo-PIV, as used in [2]. In order to scan more rapidly a volume, it is possible to use a larger laser sheet and instead of stacking images, it is possible to stack volumes reconstructed by tomo-PIV. This technique reduces the seeding density limitation of tomo-PIV and the scanning velocity limitation of scanning-PIV.

Acknowledgments

The current work has been conducted as part of the AFDAR project, Advanced Flow Diagnostics for Aeronautical research, funded by the European Commission program FP7, grant n°265695.

REFERENCES

[1] C Byrne. Block-iterative algorithms. *International Transac- tions in Operations Research*, 16(4):427–463, 2009.

[2] T. A. Casey, J Sakakibara, and S. T. Thoroddsen. Scanning tomographic particle image velocimetry applied to a turbulent jet. *Phys. Fluids*, 25:1–31, 2013.

[3] GE Elsinga, F Scarano, B Wieneke, and BW van Oudheusden. Tomographic particle image velocimetry. *Exp. in Fluids*, 41:933–947, 2006.

[4] A. Germaneau, P. Doumalin, J.-C. Dupré, L. Thomas, V. Grulier, P. Braud, B. Tremblais, and L. David. Full 3d displacement field measurement by optical scanning tomography and piv tomography. In *ICEM14*, Poitiers (France), 2010.

[5] T. Hori and J. Sakakibara. High-speed scanning stereoscopic piv for 3d vorticity measurements in liquids. *Meas. Sci. Technol.*, 15:1067–1078, 2004.

[6] J. Katz and J. Sheng. Applications of holography in fluid mechanics and particle dynamics. *Annu. Rev. Fluid Mech.*, 42:531–555, 2009.

[7] H.-G. Maas, A. Gruen, and D. Papantoniou. Particle tracking in three-dimensional turbulent flows - part i: Photogrammetric determination of particle coordinates. *Exp. in Fluids*, 15:133–146, 1993.

[8] N. Malik, T. Dracos, and D. Papantoniou. Particle tracking in three-dimensional turbulent flows - part ii: Particle tracking. *Exp. in Fluids*, 15:279–294, 1993.

[9] R. J. Moffat. Describing the uncertainties in experimental results. *Exp. Ther. Fluid. Sci.*, 1:3–17, 1988.

[10] A. Santa Cruz, L David, J Pécheux, and A. Texier. Characterization by proper-orthogonal-decomposition of the passive controlled wake flow downstream of a half cylinder. *Exp. in Fluids*, 39:730–742, 2005.

[11] F Scarano. Tomographic piv: principles and practice. *Meas. Sci. Technol.*, 24(1):1–28, 2013.

[12] F Scarano and C Poelma. Three-dimensional velocity patterns of cylinder wakes. *Exp. in Fluids*, 47:69–83, 2009.

[13] L. Thomas, B. Tremblais, and L. David. Optimisation of the volume reconstruction for classical tomo-piv algorithms (mart, bimart and smart): synthetic and experimental studies. *Exp. in Fluids*, submitted, 2013.

[14] B. Tremblais, L. David, D. Arrivault, J. Dombre, L. Chatellier, and L. Thomas. Slip : Simple library for image processing (version 1.0). http://www.sic.sp2mi.univ-poitiers.fr/slip/, 2010.